Water-Soluble Superparamagnetic Magnetite Nanoparticles with Biocompatible Coating for Enhanced Magnetic Resonance Imaging

Lisong Xiao,[†,‡] Jiangtian Li,[†,‡] Dermot F. Brougham,[§] Eoin K. Fox,[§] Neus Feliu,[⊥] Alexey Bushmelev,[∥] Annette Schmidt,[∥] Natascha Mertens,[#] Fabian Kiessling,[#] Martin Valldor,[△] Bengt Fadeel,[⊥] and Sanjay Mathur[†,*]

[†]Chair Institute of Inorganic and Materials Chemistry, University of Cologne, D-50939 Cologne, Germany, [§]School of Chemical Sciences, National Institute for Cellular Biotechnology, Dublin City University, Dublin 9, Ireland, [⊥]Division of Molecular Toxicology, Institute of Environmental Medicine, Karolinska Institutet, 17177 Stockholm, Sweden, [∥]Institute of Physical Chemistry, University of Cologne, D-50939 Cologne, Germany, [#]Department of Experimental Molecular Imaging, RWTH Aachen University, 52074 Aachen, Germany, and [△]Physics Department, University of Cologne, D-50937 Cologne, Germany. [‡]These authors contributed equally to this work.

ABSTRACT Ultrasmall superparamagnetic Fe_3O_4 nanoparticles (USIRONs) were synthesized by a novel, easily scalable chemical reduction of colloidal iron hydroxide under hydrothermal conditions. The average crystallite size (5.1 ± 0.5 nm) and good crystallinity of the samples were supported by HR-TEM analysis and the saturation magnetization value (47 emu g^{-1}). Vitamin C, used as a chemical reducing agent, also served as a capping agent in the oxidized form (dehydroascorbic acid, DHAA) to impart nanoparticles with exceptional solubility and stability in water, PBS buffer, and cell culture medium. Detailed physicochemical analysis of the USIRON suspensions provided insight into the magnetic ordering phenomena within the colloid, arising from the formation of uniform clusters displaying a hydrodynamic size of 41 nm. Phantom experiments on the contrast agent (clinical 3 T MRI scanner) revealed an enhanced r_2/r_1 ratio of 36.4 (r_1= 5 s^{-1} mM^{-1} and r_2= 182 s^{-1} mM^{-1}) when compared to the clinically approved agents. The potential of the DHAA-Fe_3O_4 nanoparticles as negative contrast agents for MRI with optimal hydrodynamic size for extended blood circulation times was confirmed by strong contrast observed in T_2- and T_2*-weighted images. The cell tests performed with primary human immune-competent cells confirmed the excellent biocompatibility of USIRONs.

KEYWORDS: magnetic nanoparticles · superparamagnetic iron oxide · magnetic resonance imaging · biocompatibility · contrast agents

Superparamagnetic iron oxide nanoparticles have emerged as one of the primary nanomaterials for biomedical applications, particularly due to their favorable magnetic properties, low toxicity, and high chemical stability.[1−3] Intrinsic magnetic properties of nanoparticles (NPs) make them a unique contrast agent for magnetic resonance imaging (MRI) in clinical diagnostics. In the past decade, tremendous efforts have been made to develop high-quality superparamagnetic NPs as safer and effective MRI contrast agents.[4−10] High-performance MRI probes require the NPs to possess a combination of properties including (i) high magnetization for effective signal enhancement, (ii) suitable size with uniform dispersion for extended blood circulation times, which then opens the possibility for passive or active targeting, (iii) surface chemistry suitable for further functionalization and/or for specific uptake and internalization in cells,[1] and (iv) dispersibility in aqueous media and biocompatibility.[8,11] In this context, a reproducible synthetic pathway to produce biocompatible and functionalizable superparamagnetic iron oxide NPs for *in vitro/in vivo* applications is highly desirable.

To fabricate iron oxide NPs, two conventional methods are commonly used: co-precipitation reactions[1,2] and high-temperature decomposition of metal−organic iron precursors[12−15] in suitable medium.[16−20] For a straightforward synthesis of water-soluble and biocompatible FeO_x NPs, co-precipitation of Fe(II) and Fe(III)-hydroxides in aqueous solution seems to be the optimal choice. However, co-precipitation reactions are thermodynamically driven (formation of an insoluble precipitate being the driving force) and do not provide good control over size distribution and crystallinity of resulting particles.[1,2,21] Recently, highly crystalline and monodispersed iron oxide NPs have been synthesized in nonaqueous media by using high-temperature decomposition reactions of metal−organic compounds. However, the FeO_x NPs produced from these methods are soluble only in organic solvents due to the

* Address correspondence to Sanjay.mathur@uni-koeln.de.

Received for review April 12, 2011 and accepted July 26, 2011.

Published online July 26, 2011
10.1021/nn201348s

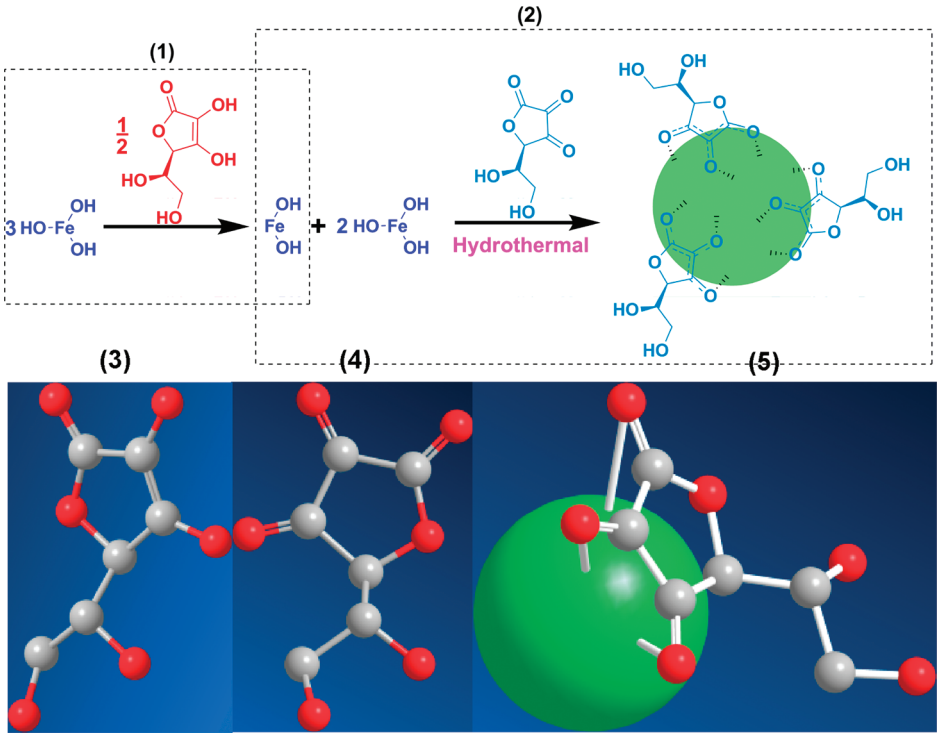

Scheme 1. Top line: Schematic representation of the preparation of USIRONs. Bottom line from left to right: 3D structures for vitamin C (3), DHAA (4), and the interaction between the iron oxide NPs and the capping agent (5). Gray, red, and green balls correspond to the carbon atoms, oxygen atoms, and iron oxide NPs, respectively.

hydrocarbon periphery of surfactants used to stabilize the NPs, and further tedious ligand-exchange procedures are required to obtain aqueous suspensions.[22−25] Therefore, the preparation of water-dispersible iron oxide NPs with appropriate surface coatings remains a significant challenge for preparative nanotechnology.

In this study, water-soluble, biocompatible ultrasmall superparamagnetic iron oxide nanoparticles (USIRONs) were prepared by the chemical reduction of $Fe(OH)_3$ colloid using a natural nutrient, vitamin C, as the reducing agent under mild hydrothermal conditions. During the synthesis, the reduction of Fe^{3+} to Fe^{2+} to form $Fe(OH)_3/Fe(OH)_2$ colloids, with a stoichiometric ratio of 2:1, was precisely controlled by the amount of added vitamin C (Scheme 1, (1)). The controllable and slow condensation of iron hydroxides provided a possibility to avoid the adverse effects on the composition, size, morphology, and magnetic properties of the NPs caused by the variation of Fe^{3+}/Fe^{2+} ratio in the traditional coprecipitation method.[1,2,21] Not only did vitamin C act as the reducing agent by oxidizing its C═C double bond, but more strikingly its oxidized product (dehydroascorbic acid, DHAA) also acted as a stabilizer and capping ligand due to the chemical interaction of its carbonyl groups with FeO_x particles[26,27] (Scheme 1, (2)). The synergy of the observed redox reactions opens up a new possibility to synthesize water-soluble and biocompatible iron oxide NPs by a simple one-step method.

Herein, we report a detailed ^{1}H NMR analysis of the DHAA-capped USIRONs (DHAA-Fe_3O_4) suspensions, undertaken to study the magnetic ordering within the colloid and the interaction between the DHAA-Fe_3O_4 NPs and the surrounding water. This detailed physicochemical analysis provides a better understanding of the potential application of the DHAA-Fe_3O_4 NPs as an efficient MRI contrast agent that is stable in biological situations. In addition, primary human macrophages were chosen to carry out the cytotoxicity tests to assess the potential *in vivo* nanoparticle−cell interactions.[11]

RESULTS AND DISCUSSION

The XRD pattern (Figure 1) of the as-prepared sample confirmed the formation of cubic Fe_3O_4 (JCPDS No. 89-0688). The average crystallite size of the individual magnetite NPs estimated from the broadening of the XRD peaks using the Debye−Scherrer formula[28] was found to be 5.6 nm. To further confirm the formation of the magnetite structure, the as-prepared sample was annealed at 250 °C for 12 h. The XRD pattern (Figure S1) of the annealed sample indicated that the γ-Fe_2O_3 was formed after the annealing and confirmed that the sample is predominantly Fe_3O_4 at room temperature.

The transmission electron microscopy (TEM) analysis (Figure 2a) confirmed that the prepared NPs have a spherical shape and narrow size distribution with an average size of about 5.1 ± 0.5 nm (for particle size distribution see Figure S2), which was consistent with the crystallite size, calculated from the XRD data. HR-TEM analysis of the samples confirmed that each particle is a well-ordered single-domain crystal

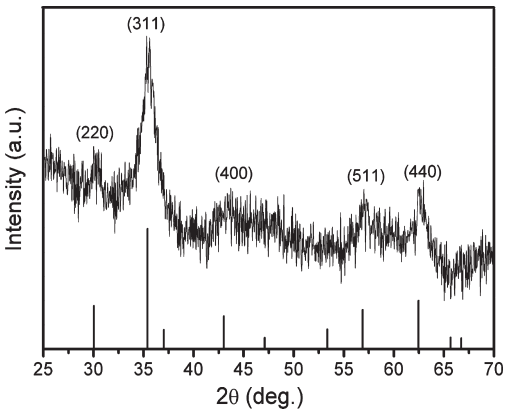

Figure 1. XRD pattern of the as-prepared iron oxide NPs. The lines correspond to the profile of the magnetic cubic phase (JCPDS No. 89-0688).

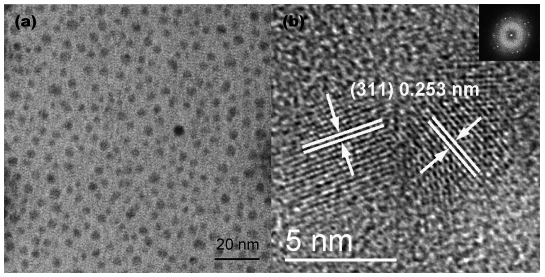

Figure 2. TEM (a) and HR-TEM (b) images of as-prepared iron oxide NPs in water. The inset in (b) is the electron diffraction pattern of the as-prepared NPs.

(Figure 2b). Measured distance between two adjacent lattice fringes gave a value of 0.253 nm, corresponding to the lattice spacing of the (311) planes of Fe_3O_4. The electron diffraction pattern inserted in Figure 2b also supported the presence of the magnetite crystal structure.

After the purification process, the as-prepared Fe_3O_4 NPs showed an excellent redispersibility in water by ultrasonication, and the obtained suspension was stable for several months without noticeable precipitation in the absence of any further surface modification or additives. Dynamic light scattering (DLS) studies revealed the average hydrodynamic size of NPs, according to the scattering intensity (d_{DLS}), in back-scattering geometry, to be 41 nm. This is significantly larger than the core size found by TEM, XRD, and magnetization data. Further, the polydispersity index (PDI) was found to be 0.12, indicating a relatively monodisperse distribution. The hydrodynamic size obtained was found to be independent of the scattering angle; measurements at a detector angle of 90° provided a value of 43 nm (Figure S3). Given the sensitivity of light scattering intensity toward particle size, the observed valued of the PDI indicated a complete absence of any larger aggregates. It was noteworthy that the hydrodynamic size of the as-prepared NPs, directly after the hydrothermal procedure, was

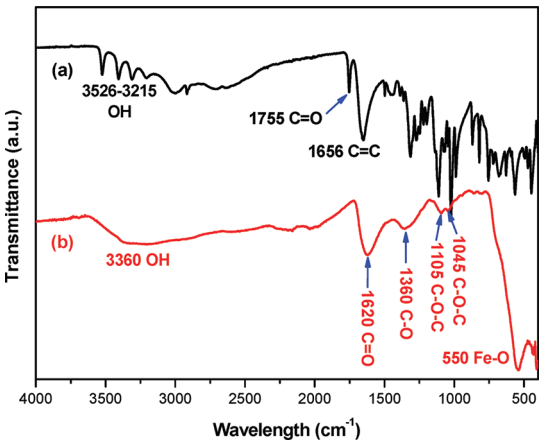

Figure 3. FTIR spectra of the vitamin C (a) and the as-prepared iron oxide NPs (b).

significantly greater (see Figure S4), which suggested that both the purification and ultrasonication steps improved the dispersibility of the DHAA-Fe_3O_4 NPs and assisted in the formation of a stable dispersion. The DLS data (size, PDI, and scattered intensity) remained unchanged over extended periods of time, within the pH range 4.7−10.1 and also for the samples prepared in 1× PBS buffer. Furthermore, the as-prepared suspensions showed long-term stability in cell culture media (RPMI + 1% penicillin/streptomycin + 10% FBS), suggesting that the suspensions are suitable for applications under physiological conditions, which is a prerequisite for biomedical applications.[16,17] The natural pH of the suspension was ca. 6.3. The zeta potential, ζ, was ca. −35 mV at pH 10 and dropped to −23 mV at pH 5. Within this range there was no observable aggregation (see Figure S5); however at pH < 4.7, a rapid precipitation of the colloid was observed. It should be noted that the DLS, zeta potential, and NMR data presented (below) were recorded for four separate dilutions taken from the original concentrated suspension. In all the cases, the d_{hyd} values obtained upon diluting samples to concentrations (1−5 mM) suitable for NMRD and DLS experiments were in the range 40−43 nm, which demonstrated an excellent shelf life of concentrated DHAA-Fe_3O_4 suspensions. The above observations indicate that DHAA-covered iron oxide NPs exhibit unusual stability and favorable colloidal properties both in aqueous suspension and in biological systems. The absence of any clustering in the TEM micrographs can be explained by the fact that the solutions used for electron microscopy were much diluted when compared to the USIRON suspensions used for NMR studies.

The chemical transformation from vitamin C to DHAA and the capping effect of DHAA on the surface of iron oxide NPs were analyzed by Fourier transform infrared spectra (FT-IR) of vitamin C, DHAA, and DHAA-Fe_3O_4 (Figures 3 and S6). Both vitamin C and DHAA have similar 3D structures, with the five-membered

ring standing in-plane with the two C—OH groups (Scheme 1). Vitamin C (Figure 3a) showed the characteristic absorption bands at 1755 cm^{-1} for C═O stretching in the five-membered lactone ring and at 1656 cm^{-1} for C═C stretching vibrations coupled with the neighboring vibrations along the conjugated system.[29,30] The DHAA derivative formed after oxidation (Figure S6) revealed strong peaks at 1790 cm^{-1} for C═O stretching due to the presence of three carbonyl groups in the DHAA ring.[29] The strong band at 550 cm^{-1} in the spectrum of the as-prepared iron oxide NPs (Figure 3b) is due to the Fe—O vibrations of magnetite NPs. However, the C═O stretching bands in vitamin C and DHAA were absent in the as-prepared NPs, which indicated that the O atom of the carbonyl group has coordinated to the Fe center on the NPs surface.[26,27,31] This coordination is further confirmed by the new absorption band at 1620 cm^{-1}. The bands at 1045, 1105, and 1360 cm^{-1} are attributed to the C—O—C and C—O stretches of the lactone ring[30] in the as-prepared DHAA-Fe_3O_4 conjugates, implying that the ring O atoms do not interact with the NPs. Furthermore, the strong OH stretching mode at 3360 cm^{-1} in the as-prepared NPs confirmed the presence of hydroxyl groups, which provided a hydrophilic component to NPs, increasing their water solubility. The exposed hydroxyl groups also present the possibility for further functionalization or binding with bioligands for biomedical applications. Thermogravimetry analysis (Figure S7) showed a weight loss due to the organic fraction corresponding to 7.3%. This is a relatively low figure, which corresponds to a footprint per DHAA molecule of only 85 $Å^2$. Considering the molecular structure of DHAA, this corresponds to submonolayer coverage. The clusters observed in suspension thus probably arise due to the aggregation of multiple USIRONs through hydrogen bonding among terminal —OH groups present on uncoated areas.

The magnetization data of DHAA-Fe_3O_4 NPs measured up to 2.2 T, at 300 K (Magnetics Vibrating Sample Magnetometer EV7), showed a hysteresis loop (Figure 4) and a saturation magnetization of 47.0 emu g^{-1} without any coercivity and remanence, demonstrating the superparamagnetic behavior of DHAA-Fe_3O_4 NPs. Taking into account the inorganic fraction only, this equates to a value of 51 emu g^{-1} for the Fe_3O_4 cores. Since the magnetization value is a function of the domain size, the saturation magnetization of the NPs, as expected, is smaller than that of bulk iron oxide.[32] Nevertheless, it is reasonable when compared to iron oxide NPs of comparable size prepared by the solvothermal and high-temperature decomposition processes.[16—19,31,33—35] The blocking temperature, T_B, was determined to be 60 K, using ZFC/FC measurements (Figure S8). Owing to the superparamagnetic behavior and good surface coverage by DHAA ligands, the NPs could be well-dispersed in the aqueous

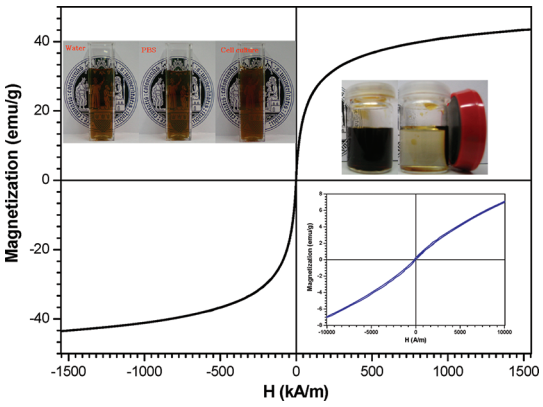

Figure 4. Hysteresis loop of the as-prepared DHAA-Fe_3O_4 NPs measured at 300 K. The left inset shows the optical images of the DHAA-Fe_3O_4 dispersions in water, PBS, and cell culture medium. The upper-right inset shows the dispersion of NPs in water before and after an external magnetic field is applied. The lower-right inset shows a close-up view of the zero crossing, confirming the absence of hysteresis.

solution without an external magnetic field (inset of Figure 4), and due to the reasonably high total magnetization, the clusters could be easily separated by applying an external magnetic field (inset of Figure 4), which is beneficial for applications such as targeted drug delivery and cell separation.

The potential of a magnetic NP suspension to enhance image contrast in magnetic resonance imaging lies in the magnetic moments of the particles, which can alter the ^1H NMR spin—lattice (R_1) and spin—spin (R_2) relaxation rates of water molecules. R_1 and R_2 are the reciprocals of the relaxation times T_1 and T_2. This effect can be used in MRI to acquire images either under T_1-weighted (positive contrast) or T_2-weighted (negative contrast) conditions. The enhancement efficiency for a given agent is quantified by the relaxivity values, r_1 and r_2, which represent the relaxation rate enhancements (relative to pure water) of the suspension, per millimolar concentration of Fe present. For DHAA-Fe_3O_4 suspensions, the measured values were $r_1 = 10.4\ s^{-1}\ mM^{-1}$ and $r_2 = 121\ s^{-1}\ mM^{-1}$ at 61 MHz, which is within the clinical MRI range (Figure 5, inset). The r_2/r_1 ratio of 11.7 is in the usable range for negative contrast applications[1] but, interestingly, is higher than expected for clusters of such relatively small size d_{hyd}.

These measurements suggest the potential of DHAA-Fe_3O_4 to occupy a useful niche in MRI. It is instructive to compare the performance (at 60 MHz) of the agents currently available or under development. In Table 1 the properties of a range of suspensions are presented in order of decreasing hydrodynamic size. There is significant ongoing interest currently in developing nanomaterials with high ratios for T_2-weighted imaging; some representative examples[22,36] are included. This approach usually involves synthesizing assemblies of larger size, in which case r_2 is enhanced by the generation of a high global cluster moment,

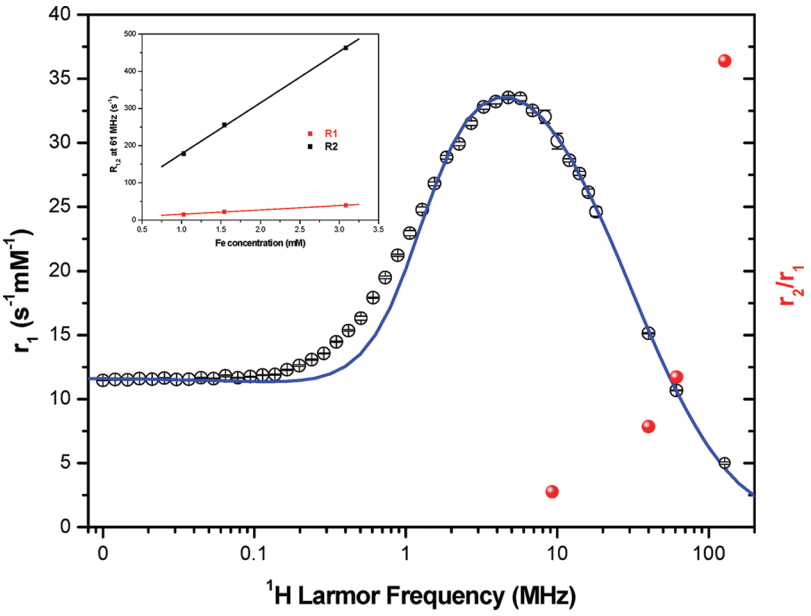

Figure 5. ^{1}H r_1 profile (○), recorded at 295 K, for a DHAA-Fe_3O_4 NP suspension, of d_{hyd} 41 nm. The solid line is the simulation generated using SPM theory. The r_2/r_1 ratio (red ●) is included on the same scale. The inset shows the concentration dependence of the relaxation rates R_1 and R_2, measured at 61 MHz; see text.

TABLE 1. Relaxometric Properties of Clinical Agents, Representative Agents from the Research Literature, and DHAA-Fe_3O_4

agent	d_{hyd}/d_{core} (nm)	r_2, r_1, (r_2/r_1) at 1.5 T, 60 MHz	coating	comment
Roig *et al.*[36]	100−300/20−60	326, 0.169 (1918)[a]	microporous silica	T_2 agent, molecular imaging
Qin *et al.*[22]	71/10.1	71, 0.31 (229)	oleic acid encapsulated with PF127	T_2 agent
Resovist	60/4.6	190, 10.9 (17.4)	carboxydextran	clinical T_2 agent (liver) T_1 possible
DHAA-Fe_3O_4	41/5.1	121, 10.4 (11.7)	DHAA	T_1 and T_2
ferumoxytol (Combidex)	30/6.4	89, 15 (5.9)	carboxymethyl-dextran	clinincal T_1 and T_2 agent, blood pool
Sinerem	15−30/4−6	65, 9.9 (6.6)	dextran	clinical T_1 and T_2 agent, blood pool
VSOP-C184	7/4	33.4, 14 (2.4)	citrate	preclinical T_1 agent, blood pool

[a] Recorded at 0.47 T, 20 MHz.

while r_1 is suppressed, largely because the NPs buried in the interior of the assembly contribute less. However, these materials are usually too large to have good blood-circulation half-lives. Resovist, with a greater d_{hyd} of ca. 60 nm, has a high ratio of 17.4,[22] but its relatively small size had also allowed it to be used for T_1-weighted imaging. The smaller agents are typically used for T_1-weighting; Sinerem (d_{hyd}, 15−30 nm) has a ratio of 6.6,[1] and ferumoxytol (d_{hyd}, ca. 30 nm) has a similar ratio to Sinerem, of 5.9.[1] At the lower end of the size range, a low r_2/r_1 ratio of 2.4 (at 60 MHz) has been reported for fully dispersed (d_{hyd}, < 10 nm) citrate-stabilized cores.[1,37] DHAA-Fe_3O_4 therefore offers a relaxivity ratio and hydrodynamic size in an intermediate range; hence it may offer simultaneous dual weighting (depending on concentration) and different biodistribution. We ascribe the high r_2 values for DHAA-Fe_3O_4 to the high global magnetic moment of the cluster,[1] which suggests that the efficient DHAA bonding and a conformal, although submonolayer, coverage allow denser packing of the particles when compared to other synthetic protocols and surface modifiers. The NMR response (Figure S9) of the suspensions was found to be unchanged in 1× PBS buffer and across the pH range of 4.7 to 10.1, within which colloidal stability was confirmed by DLS (see Supporting Information).

Currently, most comparisons of relaxometric performance are made at 1.5 T, which is within the clinical range and is reasonably accessible; however, MRI is increasingly moving to higher field for improved definition of fine anatomical features. To further evaluate the imaging properties of the particles under clinical conditions, phantom experiments were performed using a clinical 3 T MRI scanner. At this field strength relaxivities values were r_1 = 5 s^{-1} mM^{-1} and r_2 = 182 s^{-1} mM^{-1} (r_2/r_1 = 36.4). Hence the potential advantage, relative to clinically approved agents, for application as a low-d_{hyd} T_2 agent is maintained at higher field. The strong contrast deriving from DHAA-Fe_3O_4 is demonstrated in phantom experiments (Figure 6), where a strong decrease in signal intensity

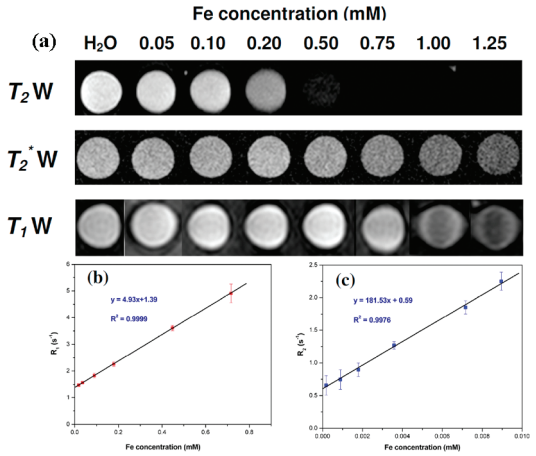

Figure 6. T_2-, T_2*-, and T_1-weighted images of DHAA-Fe_3O_4 NPs suspended in water and measured in a clinical 3 T MRI scanner (a). The Fe concentrations are indicated in mM. T_2- and T_2*-weighted images clearly demonstrate the increasing negative contrast induced by increasing concentrations of DHAA-Fe_3O_4. The plots for the r_1 and r_2 determination are shown in (b) and (c), respectively.

is observed in T_2- and T_2*-weighted images. In T_1-weighted images signal intensity increased from the Fe concentration of 0−0.5 mM. At higher concentrations the T_1-weighted signal intensity decreased again due to the strong decrease in R_2*. Nonetheless, the potential for both T_2- and T_1-weighting at reasonable concentrations is apparent. An interesting feature, illustrated in Figure 5, is the strong increase of r_2/r_1 with field. This is as expected,[1] but has not been demonstrated previously for materials in this size range.

The magnetic field-, and hence frequency-dependence, of r_1 was measured using field-cycling NMR relaxometry. This technique provides NMR dispersion curves (NMRD profiles) that can be used to assess the mechanisms that drive the NMR relaxation of the suspending solvent.[1] The profile shown in Figure 5 exhibits many of the features associated with dispersed superparamagnetic NPs: a maximum in the low MHz range and a plateau at lower frequency. However, the absence of a minimum in the midfrequency range is noteworthy. This is normally observed for fully dispersed Fe_3O_4 NPs of core size <15 nm,[38] confirming that there are weak interparticle interactions in DHAA-Fe_3O_4 samples. Nanoparticulate agents also offer the potential for molecular imaging. We estimate that in each 5.1 nm Fe_3O_4 particle there are ca. 2900 Fe atoms, while for 41 nm DHAA-Fe_3O_4 clusters there are >100 particles/cluster. The multiplier for clusters is therefore on the order of 1×10^6. This suggests very high r_1, and particularly r_2, values per mM of clusters for iron-oxide based agents in this size range.

The statistical parametric mapping (SPM) provides a numerical approach for simulating the ^{1}H r_1 profiles in suspensions of superparamagnetic nanoparticles.[39] In the high-frequency range, the particle moments are locked to the external field and relaxation is due to modulation of the dipolar interaction between the ^{1}H nuclei and the particle moment, arising from the diffusion of the solvent about the static moment. In the low-frequency range, modulation is due to the Néel process: reorientation of the moments in the local magnetocrystalline field. In the intermediate range an interpolation is performed. SPM theory has been successfully applied to interpret NMRD data for suspensions of fully dispersed NPs[37,40] and NP clusters.[41] In the former case, it has been possible to produce almost quantitative agreement with independently measured saturation magnetization values. However, the NMR particle size is found to be greater than the core size measured by TEM,[40] as the larger particles in the size distribution make a greater contribution to the relaxivity.

Application of SPM theory to NMRD data recorded for aqueous DHAA-Fe_3O_4 suspensions gave excellent agreement, with a slight discrepancy in the interpolated region. The experimental data and simulation are shown in Figure 5. The parameters used in the simulation were size $d_{NMR} = 12.5$ nm, saturation magnetization $M_{NMR} = 41$ emu g^{-1}, Néel correlation time $\tau_N = 3.3$ ns, and magnetocrystalline anisotropy energy $\Delta E_{anis} = 4.5$ GHz. As expected the d_{NMR} value is higher than the d_{XRD} and d_{TEM} values, of 5.6 and 5.1 nm, respectively. Discrepancies, as compared to TEM data, ranging from +16%[37] to +57%[40] have been reported in previous studies. The M_{NMR} value of 41 emu g^{-1} compared favorably with the M_s value of 47 emu g^{-1} obtained from magnetometry. This finding suggests that the vast majority of the NPs within the clusters contribute to the relaxation of the diffusing water molecules; that is, they are fully sensed.

The τ_N and ΔE_{anis} values of our samples are low, the latter being equivalent to $\sim 27 k_B T$ at 295 K. Nevertheless, this is higher than expected for fully dispersed cores, as was suggested by the absence of a midfrequency minimum in the profile, but is still within the superparamagnetic range.[41] This finding also clearly points to the presence of interparticle interactions. ZFC/FC measurements were performed on dried suspensions, which gave a blocking temperature (T_B) of 60 K; see Supporting Information for details. T_B values of 29 K have been reported for 5.4 nm MNPs in a polystyrene matrix where the particle dilution was sufficient to prevent interaction.[42] The elevated T_B value for slightly smaller particles further confirms the presence of interparticle interactions in the DHAA-Fe_3O_4.

In the same study,[42] MNPs of average size 5.4 nm were assembled using dendrimers containing different numbers of generations in order to study the effect of particle separation on interparticle interactions. The efficacy of the concept was demonstrated by tuning the T_B from 29 to 83 K. Using the functional dependence of T_B on particle separation reported in that paper our measured T_B value of 60 K can be used to

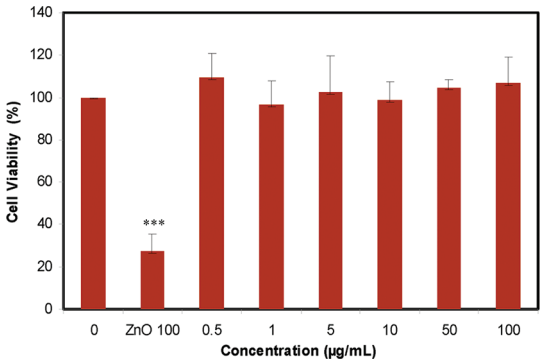

Figure 7. Cytotoxicity profile of the DHAA-Fe_3O_4 NPs for HMDM. Cell viability was assessed by LDH assay. Cells were incubated with NPs at the indicated doses for 24 h in serum-free cell culture medium. ZnO NPs were used as positive control. Results are presented as percent cell viability (mean ± SD) from 4 independent experiments using cells from different healthy blood donors. Statistical analysis was performed by one-way ANOVA followed by Tukey's *post-hoc* test. ***$p < 0.001$.

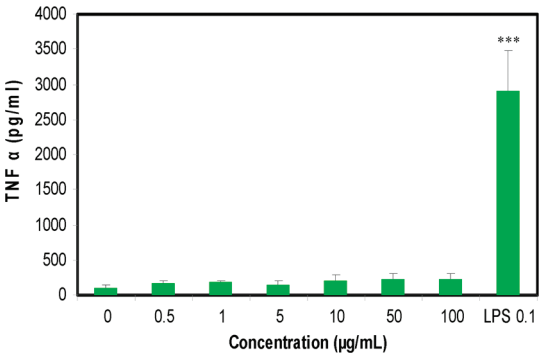

Figure 8. Pro-inflammatory cytokine secretion. HMDM were exposed to DHAA-Fe_3O_4 NPs at various concentrations for 24 h. LPS was used as a positive control. TNF-α release was assessed by ELISA. The results are presented as TNF-α release (pg/mL) (mean ± SD) from 4 independent experiments using macrophages from different healthy blood donors. Statistical analysis was performed by one-way ANOVA followed by Tukey's *post-hoc* test. ***$p < 0.001$.

estimate the interparticle separation, between the surfaces of (5.1 nm) particles within the DHAA-Fe_3O_4 clusters, at 1.8 nm. Given that the individual DHAA-Fe_3O_4 particles are slightly smaller and will thus have a reduced moment per particle, 1.8 nm can be considered an upper limit for the particle separation. The size of the DHAA molecule is known to be approximately 0.75 nm on the long axis, which is almost half the approximate interparticle separation; however caution is required when attributing physical significance to these estimates. Nevertheless, the consistent picture that emerges from considering all the physical characterization data is one of superparamagnetic ^1H solvent relaxation arising from the Fe_3O_4 NPs within small, densely packed clusters exhibiting excellent colloidal stability due to formation of a stable conformal layer of DHAA surrounding each particle within the cluster.

To assess the interaction of DHAA-Fe_3O_4 NPs with living cells, primary human macrophages in *in vitro* cell cultures were exposed to NPs. For this purpose, primary cells were selected, as they better replicate *in vivo* conditions when compared to transformed cancer cell lines.[11,43] Vallhov *et al*. have determined the importance of an endotoxin-free environment for the synthesis of NPs for biomedical applications.[44] Therefore, the DHAA-Fe_3O_4 NPs were first tested for endotoxin contamination; however, the levels of lipopolysaccharide (LPS) were found to be 8.7319 pg/mL, which is below the critical limit.[44] In a next step, the biocompatibility of DHAA-Fe_3O_4 NPs was established by exposure of primary human monocyte-derived macrophages (HMDM) to NPs followed by detection of lactate dehydrogenase (LDH) release (Figure 7). The results showed that cell viability of HMDM exposed to DHAA-Fe_3O_4 NPs was not affected. A suspension of ZnO NPs (100 μg/mL) was used as a positive control in these studies.

Certain NPs may affect immune function (for instance, cytokine secretion) in the absence of overt cell killing.[45] Therefore, to further assess the effects of DHAA-Fe_3O_4 NPs on HMDM, cells were exposed to the NPs and the secretion of tumor necrosis factor (TNF)-α, a pro-inflammatory cytokine, was determined. No cytokine secretion was seen upon incubation with DHAA-Fe_3O_4 NPs (Figure 8). However, TNF-α secretion was detected when HMDM were stimulated with bacterial LPS, as expected from previous studies.[46] This observation established that the particles do not trigger a pro-inflammatory response. In summary, the DHAA-Fe_3O_4 NP suspensions can be produced without contamination, the particles do not trigger pro-inflammatory responses in themselves, and they display excellent biocompatibility for primary human macrophages, with no evidence of nanotoxicity.

In ongoing work we are seeking to tune the core size, which we have demonstrated through the variation of synthetic temperature (Figure S10) or reaction time (Figure S11), in order to assess the effects of nanoparticle size on the magnetic and surface interactions. This would allow elucidating the control over the stability, size, and size-dispersion of clusters and also allow studying how these factors combine to determine the emergent MRI properties of the suspensions.

CONCLUSIONS

Biocompatible DHAA-Fe_3O_4 NPs suitable for forming stable aqueous dispersions were prepared by chemical reduction of $Fe(OH)_3$ using vitamin C as the reducing agent. The dehydroascorbic acid generated *in situ* as an oxidation byproduct acted as a stabilizer, under mild hydrothermal conditions. This novel and straightforward synthesis resulted in DHAA-capped superparamagnetic Fe_3O_4 NPs that exhibited high crystallinity, long-term colloidal stability, reasonable saturation

magnetization, and excellent biocompatibility as demonstrated by a cell test performed using primary human immune-competent cells. DHAA-Fe_3O_4 suspensions provided an interesting compromise between favorable colloidal properties, small hydrodynamic size and stability, and sufficient NP density to produce strong contrast in T_2- and T_2*-weighted images. As biodistribution is strongly influenced by hydrodynamic size and surface-coating properties, the DHAA-Fe_3O_4 NP suspensions described here are expected to be a promising candidate for T_2-weighted imaging, with the added possibility of useful T_1-weighting at reasonable concentrations. This potential is underlined by the very favorable results of our preliminary nanotoxicity study.

METHODS

Preparation of the DHAA-Fe_3O_4 NPs. In a typical synthesis of DHAA-Fe_3O_4 NPs, a 0.1 M $Fe(OH)_3$ colloidal solution was first prepared by adding 10 mL of a $FeCl_3 \cdot 6H_2O$ aqueous solution into 20 mL of a 0.45 M $NaHCO_3$ solution, and the obtained solution was stirred for 30 min. Subsequently, 10 mL of an aqueous solution of vitamin C in a molar ratio to Fe^{3+} of 1:6 was gradually added. The mixture was further stirred for another 10 min and then transferred into a steel-lined Teflon autoclave with a volume of 50 mL. Following this, the autoclave was kept at 150 °C for 4 h. In order to investigate the influence of reaction temperature and time on the NPs, two series of experiments have been carried out separately (110, 130, 170, 190 °C for 4 h; 150 °C for 0, 2, 6, 8 h, respectively). After the synthesis, the particles were washed three times with water and ethanol and were finally collected by centrifugation (11 000 rpm, 1 h for each time). The obtained precipitate was easily redispersible in water, PBS buffer, and cell culture medium by ultrasonication (180 s, SONOREX SUPER RK 510 H, 35 kHz, 640 W).

Characterization of DHAA-Fe_3O_4 NPs. The basic physicochemical characterizations of the DHAA-Fe_3O_4 NPs have been done by TEM, XRD, FTIR, ZFC-FC magnetization studies, and TGA analysis. TEM images were obtained on a Philips CM300 electron microscope. The phase composition of the as-prepared sample was characterized with a STOE-STADI MP X-ray powder diffraction meter operating in a transmission mode using Cu Kα (1.5406 Å) radiation. FT-IR spectra were recorded on a PerkinElmer FTIR spectrometer. The magnetization of the NPs was investigated on an ADE Magnetics vibrating sample magnetometer EV7 up to maximum field strength of 2.2 T at 300 K. Thermogravimetric analysis (TGA) was performed for freeze-dried nanoparticle samples with a TGA Q50 (TA Instruments) instrument in a flowing air atmosphere employing a heating rate of 10 °C/min. Zero-field-cooling (ZFC) and field-cooling (FC) magnetization measurements have been carried out on a dried sample with a SQUID magnetometer (Quantum Design, MPMS XL-7) under 500 Oe in the temperature range 2−300 K.

Nuclear Magnetic Resonance. The frequency dependence of the ^1H relaxation was measured over the frequency range 0.01−20 MHz using a Spinmaster FFC-2000 fast field cycling NMR relaxometer (Stelar SRL, Mede, Italy). The system operated at a measurement frequency of 9.25 MHz for ^1H. For higher frequencies (40, 61 MHz) a reconditioned Bruker WP80 electromagnet was used, with the Stelar console. T_2 was measured using the CPMG pulse sequence. At all frequencies the T_2 values were found to be independent of the echo delay used, confirming that the system is in the motionally averaged regime, which is as expected for clusters of this size.[6] All of the ^1H magnetization recovery and decay curves were monoexponential within error; the random errors in fitting T_1 and T_2 were always less than 1 and 2%, respectively. Full details of the experimental procedures are provided elsewhere.[47]

3 T MR Imaging and Relaxometry. MR imaging and MR relaxometry at 3 T (127.7 MHz) was performed in a clinical whole-body MR scanner (PHILIPS Achieva, The Netherlands) using a knee coil (SENSE-flex-M, PHILIPS, The Netherlands) at room temperature. DHAA-Fe_3O_4 water suspensions were diluted in deionized water at Fe concentrations ranging from 0.00017 to 1.25 mM. For MR measurements 0.3 mL/well of the diluted solution was filled in custom-made phantoms (Greiner 96-well flat transparent polystyrol microplate, Germany). Transverse relaxation times (T_2) were measured in 3D scan mode using multislice, multishot spin−echo sequences with 90° excitation pulses followed by a train of equally spaced 180° refocusing pulses [TR = 1500 ms, TE = 11.8 ms, number of echoes = 20, FOV = 130 × 162.5, matrix = 64 × 81, slice thickness 18 mm]. T_2 relaxation times were calculated by a linear fit of logarithmic region of interest (ROI) signal amplitudes *versus* echo time (TE). Longitudinal relaxation times (T_1) were determined using 2D multishot spin−echo sequences with a 10° excitation pulse without refocusing pulse [TR = 6.8 ms, TE = 3.3 ms, number of echoes = 1, FOV = 170 × 148.75 mm, matrix = 152 × 130, slice thickness = 5 mm]. Relaxivities r_1 and r_2 were determined by a linear fit of the inverse relaxation times as a function of the iron concentrations. Furthermore, T_1-, T_2-, and T_2*-weighted images were acquired using the following sequences: T_1-weighted turbo spin−echo (TSE) sequence [TR = 700 ms, TE = 20 ms, FOV = 150 mm, matrix = 304 × 240, slice thickness = 5 mm], T_2-weighted TSE sequence [TR = 2.0 s, TE = 40 ms, FOV = 200 mm, matrix size = 1008, slice thickness = 2 mm]; T_2*-weighted TFE imaging sequence [TR = 14 ms, TE = 5 ms, FOV = 30 mm, matrix = 144, slice thickness = 2 mm].

Determination of Iron Content. Total Fe was determined by inductively coupled plasma atomic emission spectroscopy on a Varian Liberty 220ICP. The suspension was prepared by combining a 0.2 mL aliquot of the sample with 0.5 mL of 8.8 N analar grade HCl and 1 mL of deionized water. The mixture was heated until only ca. 1 drop of liquid remained, at which time 10 mL of deionized water was added. The solution was heated to boiling and then immediately removed from the heat and allowed to cool to room temperature. The volume was adjusted to 50 mL for spectrometric analysis.

Dynamic Light Scattering. The DLS experiments were performed at 25 °C on a NanoZS (Malvern Instruments, Malvern UK), which uses a detection angle of 173° and a 3 mW He−Ne laser operating at a wavelength of 633 nm. The *z*-average diameter, d_{hyd}, and the PDI values were obtained from analysis of the correlation functions using cumulants analysis. In some cases additional measurements were made at a detector angle of 90°. Zeta potential measurements were performed at 25 °C on the NanoZS, using the M3-PALS technology.

Isolation and Culture of HMDM. Peripheral blood mononuclear cells (PBMCs) were prepared from buffy coats obtained from healthy blood donors (Karolinska University Hospital, Stockholm Sweden) by density gradient centrifugation using Lymphoprep (Axis-Shield, Oslo, Norway). Thereafter the PBMCs were positively selected for CD14 expression (CD14 MicroBeads, human, Miltenyi Biotec, Bergisch Gladbach, Germany). To obtain human monocyte-derived macrophages (HMDM), $CD14^+$ monocytes were cultured in RPMI 1640 medium (Sigma Aldrich) supplemented with 2 mmol/L L-glutamine, 100 IU/mL penicillin, 100 μg/mL streptomycin, and 10% heat-inactivated FBS, all from Gibco Invitrogen Corporation (Paisley, UK), supplemented with 50 ng/mL recombinant M-CSF (Novakemi, Handen, Sweden), for 3 days. The HMDM phenotype was confirmed by analyzing the F4/80 (Abcam, Cambridge, UK) expression using a FACscan (Becton Dickinson, Franklin Lakes, NJ, USA).

LAL Assay. The supernatant of DHAA-Fe_3O_4 NPs was controlled for LPS contamination using the LAL test method (Limulus Amebocyte Lysate (LAL) Endochrome, Charles River Endosafe, Charleston, SC, USA). The LPS levels were always below 50 pg/mL. Quantification of endotoxin in DHAA-Fe_3O_4 samples was also assessed by the LAL test.

LDH Release Assay. Release of lactate dehydrogenase to the cell culture medium of HMDM exposed to DHAA-Fe_3O_4 NPs was determined using CytoTox 96 nonradioactive cytotoxicity assay (Promega G1780, Madison, WI, USA). HMDM were plated in a 96-well plate at a density of 1×10^6 cells/mL. HMDM were exposed to particles in doses as indicated for 24 h. After exposure, 50 μL of supernatant was assayed for LDH activity following the manufacturer's protocol. The calculation of cytotoxicity percentage was as follows: % cytotoxicity = experimental LDH/maximum LDH release. The results are derived from triplicates from four independent experiments using cells from different healthy blood donors.

Cytokine Release. Cell culture supernatants from HMDM were harvested at 24 h after exposure to DHAA-Fe_3O_4 NPs or LPS (L4391 *Escherichia coli*, serotype 0111:B4, Sigma-Aldrich) at the indicated concentrations and were kept at −80 °C until cytokine analysis. ZnO NPs (Zincox10, IBU-Tec, Advanced Materials AG, Weimar, Germany) were utilized as a positive control. Tumor necrosis factor-α (TNF-α) level was measured by the ELISA kit (Mabtech, Nacka, Sweden) according to the manufacturer's instruction. The absorbance was measured at 405 nm using a spectrophotometer (Infinite F200, Tecan, Männedorf, Switzerland, or Multiskan Ascent, Thermo Scientific). Results are expressed as pg/mL ± SD of released cytokine, based on triplicates from four independent experiments using cells from different healthy blood donors. The following detection limit was considered: TNF-α < 8 pg/mL.

Statistics. Statistical significance was tested by one-way ANOVA followed by Tukey's *post-hoc* test using GraphPad Prism version 5.02 for Windows (GraphPad Software, San Diego, CA, USA). *p*-values < 0.05 were considered significant.

Acknowledgment. We gratefully acknowledge the financial support provided by University of Cologne, German Science Foundation (DFG), and European Commission (EC-FP7-NANOMMUNE-Grant Agreement No. 214281). The authors are thankful to Dr. L. Belkoura, Mr. O. Arslan from University of Cologne for the TEM measurement, Dr. H. Du from University of Bonn for the HR-TEM measurement, and Dr. S. Stucky for fruitful discussions. E.K.F. acknowledges Enterprise Ireland (Technology Development Award CFTD/2008/135) for financial support.

Supporting Information Available: XRD of annealed sample, histogram of particle size distribution, DLS intensity size distributions for DHAA-Fe_3O_4 NPs in aqueous suspension, DLS intensity size distribution (and TEM) for original NPs directly after the hydrothermal process, zeta potential over pH ranges, FTIR spectrum of DHAA, TGA of DHAA-Fe_3O_4 NPs, ZFC-FC curves, NMR data under different conditions (PBS, pH = 10.1 and pH = 5.7), XRD patterns of NPs obtained under different conditions, and DLS intensity size distributions over time. This material is available free of charge *via* the Internet at http://pubs.acs.org.

REFERENCES AND NOTES

1. Laurent, S.; Forge, D.; Port, M.; Roch, A.; Robic, C.; Vander, L.; Muller, R. Magnetic Iron Oxide Nanoparticles: Synthesis, Stabilization, Vectorization, Physicochemical Characterizations, and Biological Applications. *Chem. Rev.* **2008**, *108*, 2064–2110.
2. Gupta, A. K.; Gupta, M. Synthesis and Surface Engineering of Iron Oxide Nanoparticles for Biomedical Applications. *Biomaterials* **2005**, *26*, 3995–4021.
3. LaConte, L.; Nitin, N.; Bao, G. Magnetic Nanoparticle Probes. *Mater. Today* **2005**, *8*, 32–38.
4. Tromsdorf, U. I.; Bruns, O. T.; Salmen, S. C.; Beisiegel, U.; Weller, H. A Highly Effective, Nontoxic T_1 MR Contrast Agent Based on Ultrasmall PEGylated Iron Oxide Nanoparticles. *Nano Lett.* **2009**, *9*, 4434–4440.
5. Jun, Y.; Lee, J.; Cheon, J. Chemical Design of Nanoparticle Probes for High-Performance Magnetic Resonance Imaging. *Angew. Chem., Int. Ed.* **2008**, *47*, 5122–5135.
6. Tan, H.; Xue, J. M.; Shuter, B.; Li, X.; Wang, J. Synthesis of PEOlated Fe_3O_4@SiO_2 Nanoparticles via Bioinspired Silification for Magnetic Resonance Imaging. *Adv. Funct. Mater.* **2010**, *20*, 722–731.
7. Sun, C.; Du, K.; Fang, C.; Bhattarai, N.; Veiseh, O.; Kievit, F.; Stephen, Z.; Lee, D.; Ellenbogen, R. G.; Ratner, B.; *et al.* PEG-Mediated Synthesis of Highly Dispersive Multifunctional Superparamagnetic Nanoparticles: Their Physicochemical Properties and Function in Vivo. *ACS Nano* **2010**, *4*, 2402–2410.
8. Huang, J.; Bu, L.; Xie, J.; Chen, K.; Cheng, Z.; Li, X.; Chen, X. Effects of Nanoparticle Size on Cellular Uptake and Liver MRI with Polyvinylpyrrolidone-Coated Iron Oxide Nanoparticles. *ACS Nano* **2010**, *4*, 7151–7160.
9. Basly, B.; Felder-Flesch, D.; Perriat, P.; Billotey, C.; Taleb, J.; Pourroy, G.; Begin-Colin, S. Dendronized Iron Oxide Nanoparticles as Contrast Agents for MRI. *Chem. Commun.* **2010**, *46*, 985–987.
10. Bruns, O. T.; Ittrich, H.; Peldschus, K.; Kaul, M. G.; Tromsdorf, U. I.; Lauterwasser, J.; Nikolic, M. S.; Mollwitz, B.; Merkel, M.; Bigall, N. C.; *et al.* Real-time Magnetic Resonance Imaging and Quantification of Liporotein Metabolism In Vivo Using Nanocrystals. *Nat. Nanotechnol.* **2009**, *4*, 193–201.
11. Kunzmann, A.; Andersson, B.; Thurnherr, T.; Krug, H.; Scheynius, A.; Fadeel, B. Toxicology of Engineered Nanomaterials: Focus on Biocompatibility, Biodistribution and Biodegradation. *Biochim. Biophys. Acta* **2011**, *1810*, 361–371.
12. Sun, S.; Zeng, H. Size-Controlled Synthesis of Magnetite Nanoparticles. *J. Am. Chem. Soc.* **2002**, *124*, 8204–8205.
13. Sun, S.; Zeng, H.; Robinson, D. B.; Raoux, S.; Rice, P. M.; Wang, S. X.; Li, G. Monodisperse MFe_2O_4 (M = Fe, Co, Mn) Nanoparticles. *J. Am. Chem. Soc.* **2004**, *126*, 273–279.
14. Park, J.; An, K.; Hwang, Y.; Park, J.; Noh, H.; Kim, J.; Park, J.; Hwang, N.; Hyeon, T. Ultra-large-scale Syntheses of Monodisperse Nanocrystals. *Nat. Mater.* **2004**, *3*, 891–895.
15. Jeong, U.; Teng, X.; Wang, Y.; Yang, H.; Xia, Y. Superparamagnetic Colloids: Controlled Synthesis and Niche Applications. *Adv. Mater.* **2007**, *19*, 33–60.
16. Hu, F.; MacRenaris, K.; Waters, E. A.; Liang, T.; Schultz-Sikma, E. A.; Eckermann, A. L.; Meade, T. J. Ultrasmall, Water-Soluble Magnetite Nanoparticles with High Relaxivity for Magnetic Resonance Imaging. *J. Phys. Chem. C* **2009**, *113*, 20855–20860.
17. Wan, J.; Cai, W.; Meng, X.; Liu, E. Monodisperse Water-Soluble Magnetite Nanoparticles Prepared by Polyol Process for High-performance Magnetic Resonance Imaging. *Chem. Commun.* **2007**, *47*, 5004–5006.
18. Ge, J.; Hu, Y.; Biasini, M.; Dong, C.; Guo, J.; Beyermann, W. P.; Yin, Y. One-step Synthesis of Highly Water-Soluble Magnetite Colloidal Nanocrystals. *Chem.—Eur. J.* **2007**, *13*, 7153–7161.
19. Hu, F.; Wei, L.; Zhou, Z.; Ran, Y. L.; Li, Z.; Gao, M. Y. Preparation of Biocompatible Magnetite Nanocrzstals for *In Vivo* Magnetic Resonance Detection of Cancer. *Adv. Mater.* **2006**, *18*, 2553–2556.
20. Jia, X.; Chen, D.; Jiao, X.; Zhai, S. Environmentally-friendly Preparation of Water-Dispersible Magnetite Nanoparticles. *Chem. Commun.* **2009**, *8*, 968–970.
21. Jain, T. K.; Richey, J.; Strand, M.; Leslie-Pelecky, D. L.; Flask, C. A.; Labhasetwar, V. Magnetic Nanoparticles with Dual Functional Properties: Drug Delivery and Magnetic Resonance Imaging. *Biomaterials* **2008**, *29*, 4012–4021.
22. Qin, J.; Laurent, S.; Jo, Y. S.; Roch, A.; Mikhaylova, M.; Bhujwalla, Z. M.; Muller, R. N.; Muhammed, M. A High-performance Magnetic Resonance Imaging T_2 Contrast Agent. *Adv. Mater.* **2007**, *19*, 1874–1878.
23. Hofmann, A.; Thierbach, S.; Semisch, A.; Hartwig, A.; Taupitz, M.; Ruhl, E.; Graf, C. Highly Monodisperse Water-dispersable Iron Oxide Nanoparticles for Biomedical Applications. *J. Mater. Chem.* **2010**, *20*, 7842–7853.
24. Cheng, D.; Hong, G.; Wang, W.; Yuan, R.; Ai, H.; Shen, J.; Liang, B.; Gao, J.; Shuai, X. Nonclustered Magnetite Nanoparticle Encapsulated Biodegradable Polymeric Micelles with Enhanced Properties for In Vivo Tumor Imaging. *J. Mater. Chem.* **2011**, DOI: 10.1039/C0JM03783D.
25. Wang, Y.; Wong, J. F.; Teng, X. W.; Lin, X. Z.; Yang, H. Pulling" Nanoparticles into Water: Phase Transfer of Oleic Acid Stabilized Monodisperse Nanoparticles into Aqueous Solutions of α-Cyclodextrin. *Nano Lett.* **2003**, *3*, 1555–1559.

26. Li, Z.; Chen, H.; Bao, H.; Gao, M. One-Pot Reaction to Synthesized Water-Soluble Magnetite Nanocrystals. *Chem. Mater.* **2004**, *16*, 1391–1393.
27. Li, Z.; Wei, L.; Gao, M.; Lei, Hao One-Pot Reaction to Synthesize Biocompatible Magnetite Nanoparticles. *Adv. Mater.* **2005**, *17*, 1001–1005.
28. Xiao, L.; Shen, H.; von Hagen, R.; Pan, J.; Belkoura, L.; Mathur, S. *Chem. Commun.* **2010**, *46*, 6509–6511.
29. Kokoh, K. B.; Hahn, F.; Metayer, A.; Lamy, C. FTIR Spectroelectrochemical Investigation of the Electrocatalytic Oxidation of Ascorbic Acid at Platinum Electrodes in Acid Medium. *Electrochim. Acta* **2002**, *47*, 3965–3969.
30. Panicker, C. Y.; Varghese, H. T.; Philip, D. FT-IR, FT-Raman and SERS Spectra of Vitamin C. *Spectrochim. Acta A* **2006**, *65*, 802–804.
31. Lu, X.; Niu, M.; Qiao, R.; Gao, M. Superdispersible PVP-coated Fe_3O_4 Nanocrystals Prepared by a `One-Pot' Reaction. *J. Phys. Chem. B* **2008**, *112*, 14390–14394.
32. Aslam, M.; Schultz, E. A.; Sun, T.; Meade, T.; Dravid, V. P. Synthesis of Amine-stabilized Aqueous Colloidal Iron Oxide Nanoparticles. *Cryst. Growth Des.* **2007**, *7*, 471–475.
33. Roca, A. G.; Morales, M. P.; O'Grady, K.; Serna, C. J. Structural and Magnetic Properties of Uniform Magnetite Nanoparticles Prepared by High Temperature Decomposition of Organic Precursors. *Nanotechnology* **2006**, *17*, 2783–2788.
34. Roca, A. G.; Niznansky, D.; Poltierova-Vejpravova, J.; Bittova, B.; González-Fernández, M. A.; Serna, C. J.; Morales, M. P. Magnetite Nanoparticles with no Surface Spin Canting. *J. Appl. Phys.* **2009**, *105*, 114309–114315.
35. Demortière, A.; Panissod, P.; Pichon, B. P.; Pourroy, G.; Guillon, D.; Donnio, B.; Bégin-Colin, S. Size-dependent Properties of Magnetic Iron Oxide Nanocrystals. *Nanoscale* **2011**, *3*, 225–232.
36. Taboada, E.; Solanas, R.; Rodriguez, E.; Weissleder, R.; Roig, A. Supercritical-Fluid-Assisted One-Pot Synthesis of Biocompatible Core(g-Fe_2O_3)/Shell(SiO_2) Nanoparticles as High Relaxivity T_2-Contrast Agents for Magnetic Resonance Imaging. *Adv. Funct. Mater.* **2009**, *19*, 2319–2324.
37. Taboada, E.; Rodriguez, E.; Roig, A.; Oro, J.; Roch, A.; Muller, R. N. Relaxometric and Magnetic Characterization of Ultrasmall Iron Oxide Nanoparticles with High Magnetization. Evaluation as Potential T_1 Magnetic Resonance Imaging Contrast Agents for Molecular Imaging. *Langmuir* **2007**, *3*, 4583–4588.
38. Stolarczyk, J.; Ghosh, S.; Brougham, D. F. Controlled Growth of Nanoparticle Clusters through Competitive Stabilizer Desorption. *Angew. Chem., Int. Ed.* **2009**, *48*, 175–178.
39. Roch, A.; Muller, R. N.; Gillis, P. Theory of Proton Relaxation Induced by Superparamagnetic Particles. *J. Chem. Phys.* **1999**, *110*, 5403–5411.
40. Meledandri, C. J.; Stolarczyk, J. K.; Ghosh, S.; Brougham, D. F. Nonaqueous Magnetic Nanoparticle Suspensions with Controlled Particle Size and Nuclear Magnetic Resonance Properties. *Langmuir* **2008**, *24*, 14159–14165.
41. Corr, S. A.; Gun'ko, Y. K.; Tekoriute, R.; Meledandri, C. J.; Brougham, D. F. Poly(sodium-4-styrene) sulfonate−Iron Oxide Nanocomposite Dispersions with Controlled Magnetic Resonance Properties. *J. Phys. Chem. C* **2008**, *112*, 13324–13327.
42. Frankamp, B. L.; Boal, A. K.; Tuominen, M. T.; Rotello, V. M. Direct Control of the Magnetic Interaction between Iron Oxide Nanoparticles through Dendrimer-Mediated Self-assembly. *J. Am. Chem. Soc.* **2005**, *127*, 9731–9735.
43. Chen, Y.; Chen, H.; Zeng, D.; Tian, Y.; Chen, F.; Feng, J.; Shi, J. Core/Shell Structured Hollow Mesoporous Nanocapsules; A Potential Platform for Simultaneous Cell Imaging and Anticancer Drug Delivery. *ACS Nano* **2010**, *4*, 6001–6013.
44. Vallhov, H.; Qin, J.; Johansson, S. M.; Ahlborg, N.; Muhammed, M.; Scheynius, A.; Gabrielsson, S. The Importance of An Endotoxin-free Environment During the Production of Nanoparticles Used in Medical Applications. *Nano Lett.* **2006**, *6*, 1682–1686.
45. Braydich-Stolle, L.; Speshock, J.; Castle, A.; Smith, M.; Murdock, R. C.; Hussain, S. M. Nanosized Aluminum Altered Immune Function. *ACS Nano* **2010**, *4*, 3661–3670.
46. Witasp, E.; Kupferschmidt, N.; Bengtsson, L.; Hultenby, K.; Smedman, C.; Paulie, S.; Garcia-Bennett, A.; Fadeel, B. Efficient Internalization of Mesoporous Silica Particles of Different Sizes by Primary Human Macrophages without Impairment of Macrophage Clearance of Apoptotic or Antibody-opsonized Target Cells. *Toxicol. Appl. Pharmacol.* **2009**, *239*, 306–19.
47. Meledandri, C. J.; Ninjbadgar, T.; Brougham, D. F. Size-controlled Magnetoliposomes with Tunable Magnetic Resonance Relaxation Enhancements. *J. Mater. Chem.* **2011**, *21*, 214–222.